Toward inclusion of atmospheric effects in the aircraft community noise predictions

# Toward inclusion of atmospheric effects in the aircraft community noise predictions

Yunusi Fuerkaiti, Damiano Casalino, Francesco Avallone, et al.

Citation: The Journal of the Acoustical Society of America **150**, 759 (2021); doi: 10.1121/10.0005733
View online: https://doi.org/10.1121/10.0005733
View Table of Contents: https://asa.scitation.org/toc/jas/150/2
Published by the Acoustical Society of America

JASA ARTICLE

# Toward inclusion of atmospheric effects in the aircraft community noise predictions

Yunusi Fuerkaiti,[a] Damiano Casalino, Francesco Avallone,[b] and Daniele Ragni
*Wind Energy Department, Delft University of Technology, Delft 2629HS, The Netherlands*

**ABSTRACT:**
This paper presents an atmospheric propagation model, based on ray acoustics, that accounts for realistic weather conditions in the evaluation of the noise footprint of an aircraft. Noise sources, obtained using the Ffowcs Williams and Hawkings acoustic analogy applied to scale-resolved flow simulation data, are stored on a hemisphere surrounding the vehicle. These noise sources are propagated using a propagation model that takes into account the vertical variability of air temperature and wind velocity. The electric vertical takeoff and landing aircraft, presented by Casalino, van der Velden, and Romani [(2019). in *Proceedings of the AIAA Scitech 2019 Forum*, January 7–11, San Diego, CA, pp. 1834–1851], is used as a case study; noise footprints, obtained considering various vertically varying temperature and wind velocity distributions, are compared. It is shown that weather conditions in the acoustic wave propagation can contribute to mismatch up to 4 dBA in the illuminated zone and a significant drop in the refractive shadow zone caused by the vertical air temperature and wind velocity gradients. This work constitutes the first accomplishment in including realistic atmospheric effects in aircraft community noise prediction based on scale-resolved flow simulations. © *2021 Acoustical Society of America*. https://doi.org/10.1121/10.0005733

(Received 8 February 2021; revised 29 June 2021; accepted 4 July 2021; published online 3 August 2021)
[Editor: Kirill V. Horoshenkov] Pages: 759–768

## I. INTRODUCTION

Aircraft noise is the most significant source of adverse community reaction related to the operation and expansion of airports. Aircraft noise has often been cited as the most undesirable feature of life in the urban community because of its negative impacts on health, including annoyance (Guski *et al.*, 2017), sleep disturbance (Basner and McGuire, 2018; Nassur *et al.*, 2019), cardiovascular diseases (Van Kempen *et al.*, 2018), and altered cognitive performance among children (Evrard *et al.*, 2015). However, this is expected, particularly for urban air mobility (UAM) operations, to remain the case in most regions of the world for the foreseeable future.

The recent development of UAM has widened the usage and capabilities of electric vertical takeoff and landing (eVTOL) vehicles. Previous studies on operations of urban air vehicles in several mega-cities in the United States concluded that the scalability of existing air-traffic control systems, the availability of aviation ground infrastructure, and the acceptance of the generated noise by local communities may limit their rapid implementation (Vascik and Hansman, 2018). Various researchers and developers have highlighted aeroacoustic noise as one of the greatest challenges to the operation of urban air vehicles (Antcliff *et al.*, 2016; Holden and Goel, 2016; Seeley, 2017; Vascik and Hansman, 2017). Those vehicles are expected to be first adopted for low-altitude short-range missions over densely populated areas not usually exposed to aircraft noise (Rizzi *et al.*, 2020). Uber (Holden and Goel, 2016) declared that their eVTOL vehicles shall have a maximum noise level ($L_{Amax}$) (Ahearn *et al.*, 2016) lower than 62 dBA at an altitude of 152 m to meet public acceptance, while conventional four-seat single-rotor helicopters generate noise levels higher than 80 dBA at this altitude. Therefore, in addition to the mitigation of noise at the source, it is a necessary step to accurately model noise propagation and evaluate the impact of noise on community. The recently published report by NASA (Rizzi *et al.*, 2020) highlights the state-of-the-art of UAM noise and states that there is a need to better integrate advanced propagation tools capable of handling wind and temperature effects (refraction) and ground effects (reflection and diffraction) in community noise predictions.

To accurately model noise propagation, it is essential to include the most dominant factors. As a matter of fact, noise propagation depends on the temporal and spatial variation of the atmospheric (temperature and wind velocity gradients and fluctuations) and ground (topology, obstacles, vegetation, etc.) conditions. The former are responsible for refraction of acoustic waves and insonification of the refractive shadow zone, while the latter affect the reflection and diffraction of acoustic waves (Salomons, 2001).

Noise-power-distance (NPD) data (ECAC, 2016), which are specific to each aircraft, have been widely used to evaluate aircraft noise footprint. NPD estimates noise levels for a specific aircraft type, at a given flight condition, e.g., hover, and distance from the observer. In the absence of NPD, most of the approaches adopted to evaluate aircraft noise for different flight trajectories and operating conditions start from the sampling of noise sources over a

[a]Electronic mail: y.fuerkaiti@tudelft.nl
[b]ORCID: 0000-0002-6214-5200.

hemisphere surrounding the aircraft. This approach has been widely used in recent years (Casalino *et al.*, 2019a; Conner and Page, 2002; Gervais *et al.*, 2010; Gopalan, 2004; Greenwood, 2011, 2017; Guntzer *et al.*, 2009; Lucas and Marcolini, 1997; Yin *et al.*, 2007). The noise sources are then propagated on the ground, often making the assumption of constant weather conditions, i.e., no variation of air temperature and wind velocity both in the vertical and streamwise direction. However, several studies (Browne *et al.*, 2004; Munt *et al.*, 2001; Parry *et al.*, 2020) have shown that atmospheric refraction effects are not negligible for source-receiver distance larger than 450 m. This paper focuses on the effect of atmospheric refraction due to the temperature and wind velocity gradients.

Existing propagation methods show limitation in including atmospheric and ground effects. For instance, the fast field program (FFP) (Franke and Swenson, 1989) can account only for stationary source, layered atmosphere, and a homogeneous ground surface. Methods based on a parabolic equation (PE) (Gilbert and White, 1989) are not optimal when considering moving sources (Ghinet *et al.*, 2019) and are computationally demanding for the high-frequency range. On the other hand, methods based on the solution of wave equations using discretized versions of partial differential or integral equations, typically referred to as wave-based methods, are able to include these variations, but they are prohibitively computationally expensive. Only a few examples are available restricted to relatively low-frequency problems (Casalino *et al.*, 2011, 2019b). Contrary to the aforementioned methods, ray-tracing is a widely used approach for studying sound propagation in a complex environment. The ray-tracing method hypothesizes the existence of wavefronts and the presence of rays that provide a spatial depiction of sound travel and energy flow (Lamancusa and Daroux, 1993). Ray-tracing has been shown to provide comparable results to wave-based methods for high-frequency problems. For long-range propagation, ray-tracing is preferable over wave-based methods as it demands less computational cost. Nonetheless, it is prone to numerical artifacts, such as perfect shadow zone and caustics (Ostashev and Wilson, 2015; Salomons, 2001). Shadow zone appears typically in an upward refracting atmosphere where the source-receiver range is several times longer than the source height. To correct for this numerical artifact, a correction model developed by Arntzen *et al.* (2012) is applied to approximate sound levels in the shadow zone. The correction method was developed based on the FFP. Noise levels in the shadow zone were estimated with a linear loss parameter (dB per meter). The parameter depends on the strength of the temperature and wind velocity gradients and the source frequency. This method provides an estimate of the sound levels at the transition from the illuminated zone to the shadow zone, and it predicts the additional propagation within the shadow zone.

The work of Hartjes and Visser (2019) represents an attempt to incorporate atmospheric effects on the noise footprint prediction of a helicopter. They employed the noise hemisphere approach along with a two-dimensional ray-tracing model based on Snell's law of refraction. The model is limited to cases with linear sound speed profiles. However, several studies (Klug, 1991; Panosfsky and Dutton, 1984; Stull, 1988) reported that realistic weather profiles are better characterized by logarithmic and power-law profiles. Moreover, the work did not address the variation of the source emission point on the hemisphere, i.e., ray-hemisphere intersection point, as a result of source motion and atmospheric refraction effects.

The present study extends the work of Casalino *et al.* (2019a) to include the atmospheric refraction effects when adopting a noise hemisphere database (NHD) approach for storing the noise sources. Under realistic atmospheric conditions, wind velocity and temperature gradients introduce two new physical modifications to the NHD-based noise footprint prediction approach: (i) the ray-hemisphere intersection point will be shifted at a different position; (ii) the path length of a ray between the source and the receiver becomes longer. The objective of this paper is to address these effects by coupling the NHD-based noise footprint simulation approach with a propagation model based on ray-tracing and apply it for noise prediction with realistic weather conditions and to discuss the physical improvements. The propagation model presented in this paper is a two-point three-dimensional (3D) curved ray-tracing model that incorporates the weather effects either by directly reading available weather data or by approximating the weather profiles by a known analytical profile. Two weather conditions that may appear on typical summer days are considered: clear day and clear night with different wind velocities. Finally, it is worthwhile to highlight that existing methods are implemented and combined in a framework that has not been used previously. Moreover, the presented methodology is not restricted to a specific aircraft type. Instead, it can be applied to any aerial vehicle for community noise assessments.

The remainder of this paper is structured as follows. In Sec. II, the numerical approach is described. In Sec. III, the atmospheric refraction effects on the noise footprint are studied within a case study. Finally, in Sec. IV, a summary of the work is given.

## II. NUMERICAL APPROACH

A standard hybrid approach is used to predict the source noise levels as well as the on-ground noise footprint of an aircraft. First, the unsteady flow solution around the vehicle is computed using the lattice–Boltzmann/very large eddy simulation (LB/VLES) method. In the second step, narrowband noise (NBN) spectra, retrieved from a time signal obtained from the Ffowcs Williams and Hawkings (FW-H) approach, are computed for the prescribed flight conditions at microphone locations distributed on a hemisphere around the vehicle and stored in the NHD. On-ground noise footprint is then computed using the method described below.

https://doi.org/10.1121/10.0005733

### A. Source noise prediction

The unsteady flow simulation is performed using the LB/VLES solver SIMULIA PowerFLOW®. A mathematical framework of the lattice–Boltzmann (LB) method was established by Shan *et al.* (2006).

The noise, i.e., tonal noise in terms of thickness, loading, and quadruple source, signals at locations corresponding to microphones distributed on a hemisphere around the vehicle are obtained by using the FW-H module of SIMULIA PowerACOUSTICS®. A retarded-time solution of the FW-H equation (Farassat and Succi, 1982) is used, and the time integration is carried out by employing a forward-time algorithm (Casalino, 2003). The permeable integration is performed on multiple cylinders encapsulating the vehicle, thus including the direct non-linear contribution of quadruple surfaces in the volume of fluid around the vehicle. The cylinders are cap averaged to filter out the larger vortical structures from the wake of the vehicle. The broadband noise is predicted by the intrinsic computational aeroacoustic nature of the LB method. Discussing the accuracy of the source noise prediction is beyond the scope of this paper. However, it is worth mentioning that SIMULIA PowerFLOW has already been used in the past for a variety of aircraft aeroacoustic problems and at various degrees of complexity, from component level to full vehicle. Relevant to the present study are benchmark studies conducted for rotating devices [see Casalino *et al.* (2019a) and Casalino *et al.* (2019b) for references].

### B. Extension of the NHD to a non-homogeneous moving atmosphere

When the atmosphere is homogeneous and motionless in terms of temperature and velocity, an observer sees a wavefront described by $\tau(\boldsymbol{R}) = t$ as a surface that moves with a speed $c\boldsymbol{n}$, where $t$ is time, $\boldsymbol{n}$ is normal to the wavefront, and $c$ is the local sound speed. However, when the air moves with velocity $\boldsymbol{v}$, the wavefront has local speed equal to $d\boldsymbol{R}/dt = \boldsymbol{v}_{ray} = \boldsymbol{v} + c\boldsymbol{n}$. As a consequence, the ray path vector $\boldsymbol{R}$ follows the direction of $\boldsymbol{v}_{ray}$ instead of $c\boldsymbol{n}$. Figure 1 shows the difference between the ray velocity $\boldsymbol{v}_{ray}$ and the wavefront vector $\tau(\boldsymbol{R})$ when the medium in which sound propagates is in motion. This work uses the 3D ray-tracing equation derived by Pierce (2019) that explicitly incorporates wind velocity, temperature, and their gradients.

The 3D acoustic ray-tracing system reads

$$\left.\begin{aligned} \frac{dR_i}{dt} &= \frac{c^2 s_i}{\Omega} + v_i \\ \frac{ds_i}{dt} &= -\frac{\Omega}{c}\frac{\partial c}{\partial R_i} - \sum_{j=1}^{3} s_j \frac{\partial v_j}{\partial R_i} \end{aligned}\right\}. \tag{1}$$

Here, $R_i$ is the ray path vector and $v_i$ is the medium velocity in the Cartesian coordinate system. The derivation of Eq. (1) and the relationships between wave-slowness vector $\boldsymbol{s}$, the unit normal vector to the wavefront $\boldsymbol{n}$, and the parameter $\Omega$ are given in Pierce (2019). Equation (1) is solved using a fourth-order Runge–Kutta scheme. A user defined number of time steps is used to march the solution forward in time. To obtain the eigenray that connects the source to the receiver, the ray shooting angles shall be optimized such that the ray can land at the given receiver location. In this work, the Nelder–Mead simplex-based function minimization algorithm (Nelder and Mead, 1965) is used for this purpose. A simplex is a geometrical figure that consists of $N$ dimensions of $N + 1$ vertices and all their interconnecting line segments, polygonal faces, etc. In two dimensions, a simplex is a triangle, and in three dimensions, it is a tetrahedron. A view of the algorithm is provided by Lagarias *et al.* (1998). In the proposed propagation model, the distance $D$ between the end point of a ray and a receiver position, as illustrated in Fig. 2, is the function to minimize. This implies that the elevation angle and azimuthal angle are the two variables to be optimized.

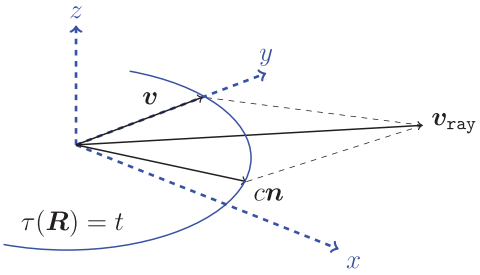


FIG. 1. (Color online) Wave normal, wind velocity, and ray path vector for a moving atmosphere.

The eigenray computation procedure in the NHD-based noise footprint prediction framework is illustrated in Fig. 2. For each source and receiver position, the direct and ground reflected eigenrays are computed with the following steps. First, the procedure starts with the initial simplex. Unlike the eigenray search strategies outlined in de Moraes Calazan and Rodríguez (2018), in this study, a rather simpler approach is used to create the initial simplex. Namely, the shooting angles from the straight rays in a constant atmosphere are used to construct the initial simplex. Next, the objective function $D$, which depends on the shooting angles, is evaluated at each vertex of the simplex. Based on the function values, one of the simplex operators known as

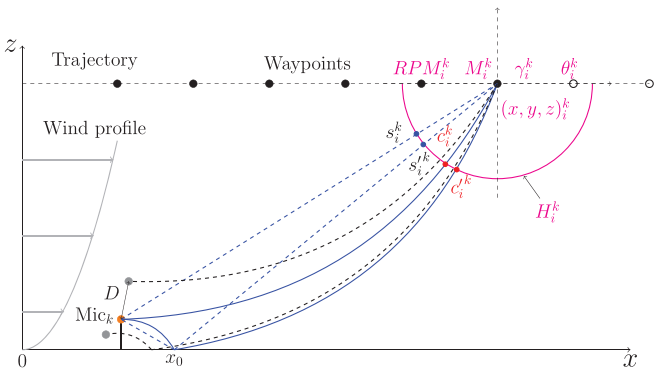


FIG. 2. (Color online) Illustration of the curved-ray NHD-based noise footprint calculation procedure for the present study.

reflection, expansion, contraction, and shrink is applied. If the function value at the new vertex is smaller, i.e., $D_{i+1} < D_i$, then a new simplex will be formed, and one of the simplex operators will be applied again. The whole process continues iteratively until the function satisfies the minimum termination criteria $\epsilon$.

For a given vehicle configuration and trajectory, computation of the on-ground noise footprint follows similar steps as NHD-based noise footprint prediction with a straight ray. For a typical eVTOL, the NHD is characterized by four parameters: flight Mach number, angle of attack, tilt angle of the rear rotors, and rotational speed of the four rotors. For fixed-wing aircraft and helicopters, the parameters would be less than four, e.g., for helicopters, advance ratio, rotor thrust, and tip-path-plane angle are sufficient to characterize the noise hemispheres for steady and unsteady maneuvers (Gennaretti *et al.*, 2016). A flight envelope is treated by considering different combinations of those parameters. Each combination represents a noise hemisphere for which an unsteady flow solution is carried out to compute the noise signals on the microphones distributed on it. NBN spectra are computed subsequently and stored in the NHD.

In this work, a single flight condition that represents a cruising flight is considered, and the noise footprint calculation procedure is displayed in Fig. 2. For every microphone $k$ on a ground surface and for every time window $i$ of 0.5 s duration, the emission time position of the vehicle along its trajectory is found. At this position, the glide angle $\gamma_i^k$ and the Mach number $M_i^k$ are calculated from the coordinates of the waypoints, whereas the pitch angle $\theta_i^k$, the rotor $RPM_i^k$, and the rear rotor tilt angles $\phi_i^k$ are interpolated from the closest waypoints. Afterward, the angle of attack $\alpha$ is estimated by subtracting the pitch angle from the glide angle ($\alpha_i^k = \theta_i^k - \gamma_i^k$). The noise hemisphere corresponding to this point of the trajectory $(x, y, z)_i^k$ is used to interpolate the corresponding noise hemisphere $H_i^k$ from the three closer conditions stored in the NHD. Finally, the propagation model with the two-point 3D eigenray tracing procedure is applied, and the ray-hemisphere intersection point for direct ray $c_i^k$ and for the reflected ray $c_i'^k$ are determined subsequently. The atmospheric refraction changes the ray-hemisphere intersection point, e.g., the point $s_i^k$ is shifted to the point $c_i^k$ on the hemisphere, and the straight eigenray paths (dashed blue lines) are replaced by the curved eigenray paths (continuous blue lines). After that, the NBN levels are interpolated at $c_i^k$ and $c_i'^k$ from the closest points on the hemisphere. It is worth highlighting that in this work the ground reflection is performed by computing the curved-ray path and ground plane intersection point, e.g., $x_0$ in Fig. 2, and updating the wave-slowness vector based on the boundary conditions at $x_0$.

The present propagation model has an advantage over the image source method to handle multiple reflections over a surface as the sound ray can be traced continuously for a given time period. Finally, the ground noise levels are calculated using the direct and reflected eigenray paths, atmospheric absorption according to the standard procedure SAE ARP 866 A, Doppler shift, and amplitude corrections.

## III. CASE STUDY

In the present study, the eVTOL vehicle described in Casalino *et al.* (2019a) is considered. The eVTOL vehicle is driven by eight 1.17 m radius propellers, which contra-rotate to maintain balance and stability. The front propellers are activated during takeoff and landing procedures. The rear propellers are shrouded, and they feature a variable tilt-angle depending on the flight conditions. The total wingspan is 15 m long, while the full fuselage length $L$ is approximately 7 m. This research considers only the cruising segment of the whole flight envelope. This indicates that only one operating condition is used to sample the source noise hemisphere, and it is used along the entire flight path. The operating conditions are flight Mach number equal to 0.2 and rotor speed rpm equal to 1500. Noise hemisphere corresponding to these conditions is obtained from the NHD in Casalino *et al.* (2019a).

The noise hemisphere is defined in the vehicle reference system (zero pitch, yaw, and roll). The hemisphere radius $R_h$ is set to 9 times the length of the fuselage to disregard the weather effects within the hemisphere. The hemisphere and the noise source distribution for the case under investigation are shown in Fig. 3.

The flight trajectory starts from point S (5, 0, 2) km and terminates at point T ( –5, 0, 2) km. To investigate the weather effects on the noise footprint at different aircraft positions, two control points, A (4.5, 0, 2) km and B (3, 0, 2) km, are set on the trajectory.

The model outputs the A-weighted OASPL for microphones located in a 6 km square area discretized by $21 \times 21$ grid points on a hard ground plane. Two different wind directions are considered: against the flight direction pointing to the positive $x$ axis, i.e., the east (E), and along the flight direction pointing to the negative $x$ axis, i.e., the west (W). An illustration of the computational scenario is shown in Fig. 4.

The vertical wind and temperature profiles are defined using the analytical formulas based on the Monin–Obukhov similarity theory (MOST) (Ostashev and Wilson, 2015; Panosfsky and Dutton, 1984; Stull, 1988). The vertical profiles are approximated by dimensional variables, such as surface roughness, friction velocity ($u_*$), and sensible heat flux ($Q_H$). The surface roughness is set to 0.01 m, which represents flat ground with short grass. For typical summer days, representative values of the friction velocity $u_*$ for light, moderate, and strong wind conditions can be selected as 0.1, 0.3, and 0.6 $\mathrm{ms}^{-1}$. For sunny conditions during the daytime, $Q_H = 200\ \mathrm{Wm}^{-2}$. For clear sky at night with moderate or strong wind, $Q_H = -20\ \mathrm{Wm}^{-2}$. Based on these parameters, two different weather conditions are considered: clear day and clear night. To investigate whether wind velocity or temperature is the dominant factor in the formation of the refraction for a specific weather condition, different friction

https://doi.org/10.1121/10.0005733

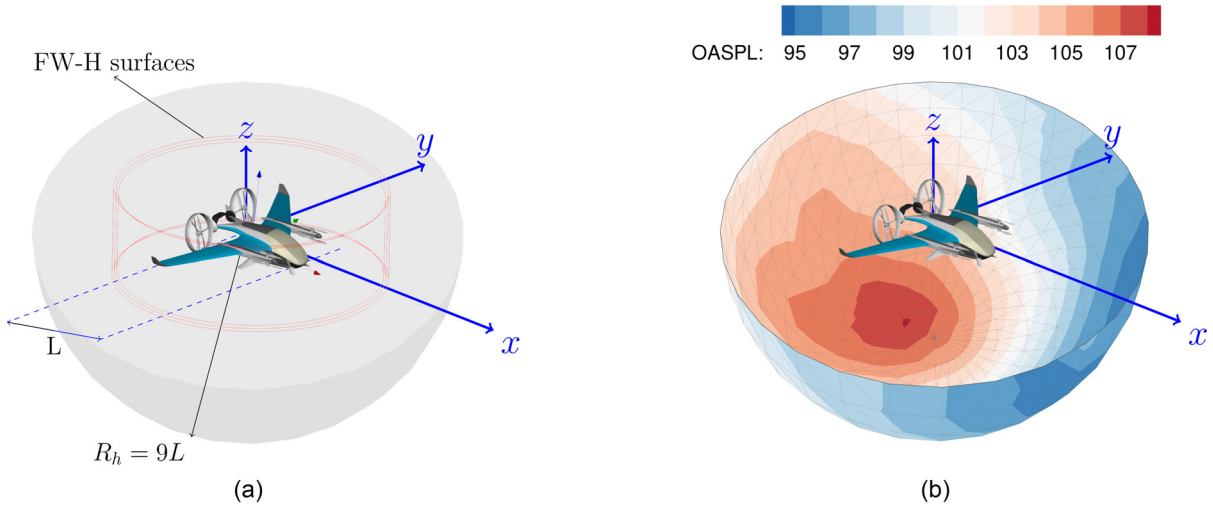


FIG. 3. (Color online) (a) 3DS (Vélizy-Villacoublay, France) eVTOL model for forward flight, including the permeable sampling surfaces for FW-H acoustic propagation and the noise hemisphere. (b) Overall sound pressure levels (OASPL) over the noise hemisphere.

velocities are selected for both weather conditions. The selected values for these weather conditions are listed in Table I, and the weather profiles are illustrated in Fig. 5.

## A. Validation

In this section, the two-point 3D eigenray tracing implementation is validated. Then a test case is used to demonstrate the accuracy of the curved-ray NHD approach in the footprint prediction.

### 1. Validation of the propagation model

The ray-tracing propagation model is initially validated against an exact solution (Salomons, 2001) that describes the elementary sound propagation problem in a homogeneous atmosphere where noise levels at the receiver locations are determined with the direct and ground reflected ray path lengths. Then the model is validated against a Gaussian beam tracing (GBT) (Gabillet *et al.*, 1993) solution for the same problem in a non-homogeneous atmosphere. A monopole source is located at (0, 0, 20) m, and all the receivers are distributed along with the horizontal range with a distance of 2 m. The receivers' height is 10 m. The maximum propagation distance along the x-axis is set to 200 m to ensure that there are only two contributing rays, i.e., one direct ray and one ground reflected ray. The source frequency is 100 Hz. The non-homogeneous atmosphere is represented with a linearly increasing sound speed profile with a sound speed gradient of $0.5\,s^{-1}$.

The eigenray tracing model result, labeled "Ray" in Fig. 6(a), is compared with the exact solution for a point source above the rigid boundary and calculations from the GBT. The only difference is an over-prediction of GBT near the source likely due to the far-field approximation inherent to the GBT. For the non-homogeneous atmosphere with a linear sound speed profile [Fig. 6(b)], the interference pattern is shifted. The ray-tracing result and GBT still show good agreement. On the basis of the results shown in Fig. 6(a), it is likely that the ray-tracing approach is more accurate near the source and is able to capture the interference shift.

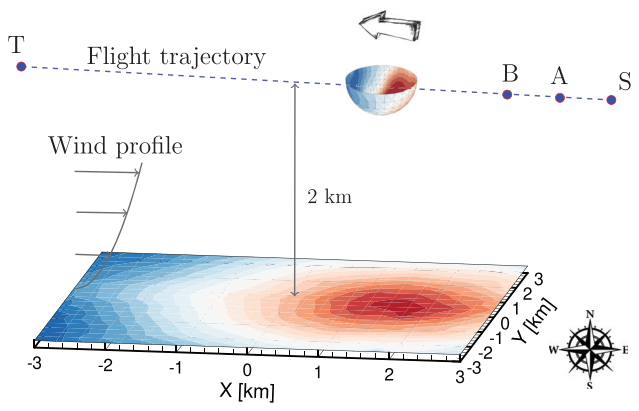


FIG. 4. (Color online) Geometry of the problem.

### 2. Accuracy of the curved-ray NHD approach

The accuracy of the ray-hemisphere intersection point and the travel time along an eigenray path is determined by the number of time steps that were used to march the ray-tracing system [Eq. (1)] solution forward in time. Namely, as outlined in Sec. II, a ray path with a larger number of time steps results in a smaller $D$ as the ray path is

TABLE I. Selected values of sensible heat flux and friction velocities for the weather conditions.

| Weather conditions | $Q_H$ ($Wm^{-2}$) | $u_*$ ($ms^{-1}$) |
|---|---|---|
| Clear night | −20 | 0.5 |
| Clear day | 200 | 0.27 |

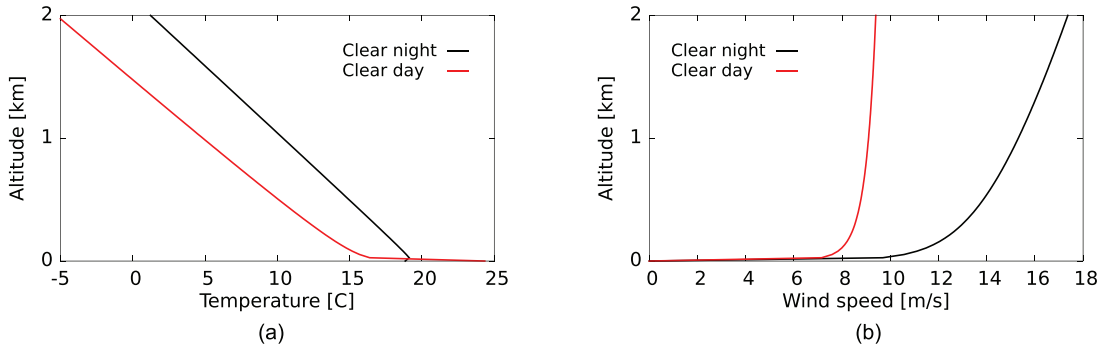


FIG. 5. (Color online) Weather profiles. (a) Temperature profiles. (b) Wind profiles. The wind direction points to the positive $x$ axis.

characterized by many points. Once $D$ is small enough, e.g., in a constant atmosphere, the ray-hemisphere intersection point and the travel time along the ray path will converge to the ray-hemisphere intersection point and travel time computed with the straight-ray NHD approach. In this subsection, the accuracy of the propagation model is investigated for cases with and without weather effects. For the case without weather effects, the straight-ray NHD is correct and used as a reference. Therefore, the flyover noise predicted with the curved-ray NHD for the different number of time steps is compared against the one predicted with the straight-ray NHD. The weather is characterized by stationary air with constant temperature of 287 K. For the case with weather effects, the curved-ray NHD with a larger number of time steps is used as a reference. The flyover noise predicted with a smaller number of time steps is compared against the one computed with a subsequent larger number of time steps. The clear day condition with the wind blowing along the flight direction is considered.

The mean absolute error (MAE) at the microphone located at the center of the ground area is calculated for the different numbers of time steps and depicted in Fig. 7. It is seen that MAE is decreasing with the increasing number of time steps. It is found that independent of the conditions, the curve starts flattening for a total number of time steps larger than 1000. In the following, the number of time steps is set to 1200 to keep the MAE below 0.2 dBA.

## B. Results

### 1. Clear night

To investigate the effects of the wind velocity and temperature gradients on sound propagation path, sound rays are traced between vehicle emission time positions and the microphones located at the corners and the center of the ground area. The vehicle emission time positions are sampled at three different waypoints, i.e., the starting point, middle point, and terminal point of the trajectory. For convenience, those emission time positions are labeled as first, second, and third emission time position.

Figure 8(a) illustrates how sound rays are refracted when the vehicle flies against the wind direction. For the microphones located at the farthest corners of the ground area, sound rays emitted from the first and second emission time positions (black and blue rays) are refracted upward before they reach the microphones. This condition results in a refractive shadow zone. When the vehicle flies in the same direction as the wind, all sound rays tend to be straight despite the presence of the weather conditions as shown in Fig. 8(b). It is worth noting that, if the vehicle flies against the wind direction, sound rays curve more when the vehicle is farther away from the microphones, and they become almost straight when the vehicle is closer to the microphones. This implies that weather has an effect on the refraction of the sound rays only if the vehicle is at a distant location.

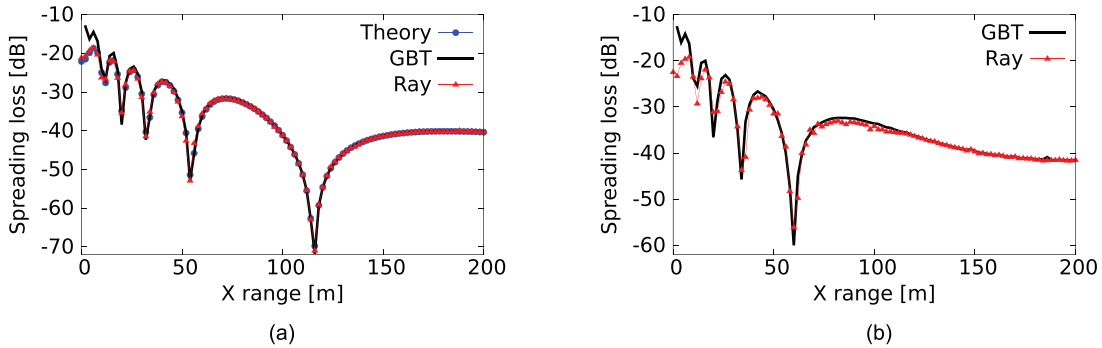


FIG. 6. (Color online) Comparison between the spreading loss calculated with different methods. (a) Homogeneous atmosphere. (b) Non-homogeneous atmosphere.

https://doi.org/10.1121/10.0005733

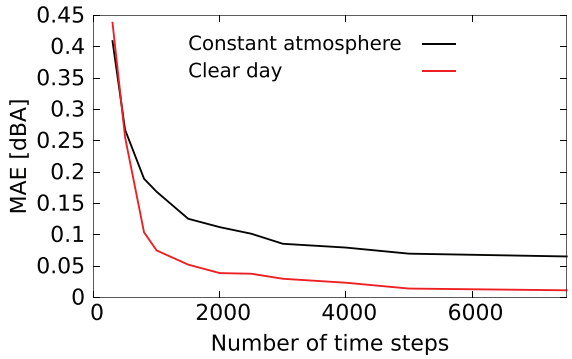


FIG. 7. (Color online) MAE as a function of the number of time steps for the cases with and without weather conditions.

To better illustrate this aspect, the on-ground noise footprints when the vehicle is located at control points A and B are displayed in Fig. 9. The loss in the refractive shadow zone is calculated by adding the loss estimated with the correction model Arntzen *et al.* (2012) to the loss at the shadow zone boundary.

When the vehicle flies against the wind direction and is located at A, due to the refractive shadow zone, noise levels start to drop rapidly after $x = -0.7$ km along the flight direction. In contrast, when the vehicle flies along the wind direction, no significant refraction effect in the noise levels is observed. The field difference between these two conditions, shown in Fig. 9(a), further highlights the relevant effect of the shadow zone; when the vehicle is at A, there is up to 24 dBA difference in the refractive shadow zone and up to 4 dBA in the illuminated zone between noise footprints computed for these two wind directions. When the vehicle flies against the wind and is positioned at B, the shadow zone boundary shifts from $x = -0.7$ km to $x = -2$ km. When the vehicle flies along the wind direction, no significant weather effects on the noise footprint are observed. The field difference between these two wind directions is plotted in Fig. 9(b). It shows that there is still up to 12 dBA difference due to the strong wind.

### 2. Clear day

The effect of the clear day condition on the sound propagation with two different wind directions is shown in Fig. 10. When the vehicle flies against the wind direction, only the sound rays traced between the farthest microphones and the first emission time positions are refracted upwards, thus causing the refractive shadow zone. For the case where the vehicle flies along the wind direction, the longest eigenrays (black and blue rays emitted from the first emission time position) are refracted slightly upward despite the wind velocity. This implies that the temperature gradient is the dominant variable that affects the refraction.

On-ground noise footprints at the control point A and B for the two wind directions are shown in Fig. 11. When the vehicle flies against the wind and is located at A, compared to the condition on the clear night, the shadow zone boundary is shifted from $x = -0.7$ km to $x = -1.8$ km along the flight direction. When the vehicle flies in the same direction as the wind, no significant weather effects on the noise footprint are seen. The difference between these two noise footprints is displayed in Fig. 11(a). It indicates noise levels drop up to 15 dBA in the refractive shadow zone and up to 3 dBA in the illuminated zone. At B, the on-ground noise footprints computed for the two wind directions showed a very similar trend. The field difference between these two conditions is shown in Fig. 11(b). This shows the difference is minimal and the shadow zone is about to disappear completely.

## IV. CONCLUSION

A new noise footprint prediction is proposed to simulate the noise footprint of an eVTOL vehicle that is cruising over flat terrain under realistic weather conditions. The meteorological effects on the on-ground noise footprint are studied with a propagation model based on the ray acoustics that is implemented in the NHD-based footprint prediction approach. For all weather conditions, on-ground noise footprints are computed. It is observed that the refractive shadow zone appears when the vehicle flies against the wind direction. The refractive shadow zone is stronger when the vehicle is farther away from the receivers and becomes weaker or disappears when the vehicle is closer to the receivers. When the vehicle flies along the wind direction, for all weather conditions, no significant weather effect on

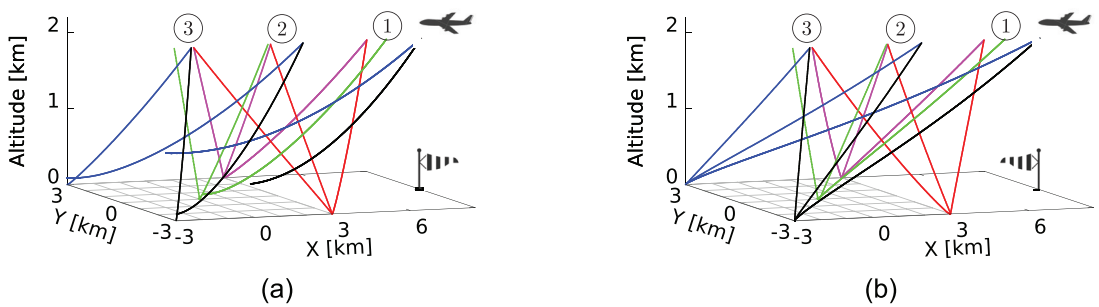


FIG. 8. (Color online) Direct eigenrays traced between vehicle emission time positions and the microphones located at the corners and the center of the ground area in the clear night condition for the wind blowing against the flight direction (a) and along the flight direction (b).

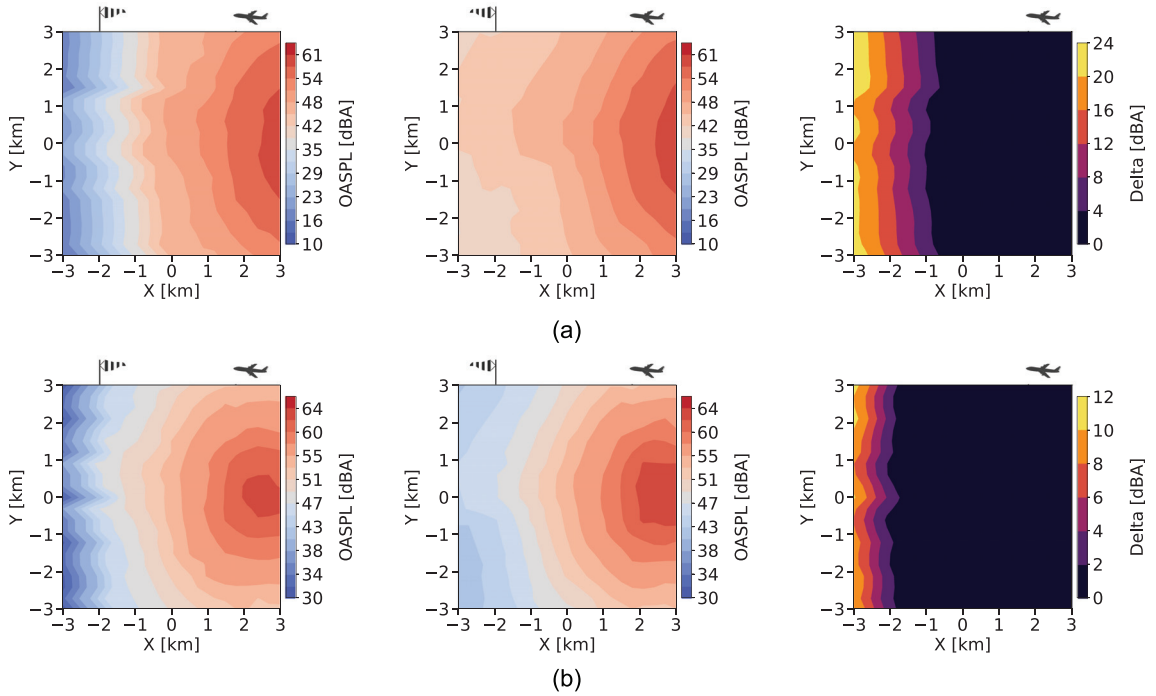


FIG. 9. (Color online) On-ground noise footprints at control point A (a) and B (b) in the clear night with wind directions against the flight direction, along the flight direction, and field difference between them.

the noise footprint is observed. Comparing the influences of different meteorological conditions on the noise footprint, the effect of the refractive shadow zone is the most relevant for the clear night condition, i.e., the case with the higher temperature and wind velocity gradients compared to the other conditions.

Some limitations in the present methodology should be recalled. For preliminary assessment, flat terrain as a perfect reflector is considered and the weather profiles obtained using MOST are used as a first approximation. However, in a realistic urban environment, temperature and wind velocity gradients are highly affected by local urban geometries and they become range dependent; therefore, complex phenomena due to the combined effect of refraction, diffraction, multiple reflections, and their dependence on the propagation range would occur during the sound propagation. More comprehensive models evaluating the complex phenomena that would appear during the sound propagation in urban settings must be developed for more realistic scenarios. Besides, a simple linear model is applied to estimate the propagation loss in the refractive shadow zone. In addition, the influence of atmospheric turbulence on the propagation is ignored. More sophisticated models are needed to describe insonification of the refractive shadow zone due to sound scattering by the atmospheric turbulence.

In the future, advances in atmospheric sciences should lead to more reliable, higher-resolution numerical weather data. Complex terrains, with changes in the ground characteristics, topography, and the effects of local meteorological conditions could be accounted for. Thus, the present study is only one step toward the inclusion of atmospheric effects in aircraft noise long-range propagation predictions.

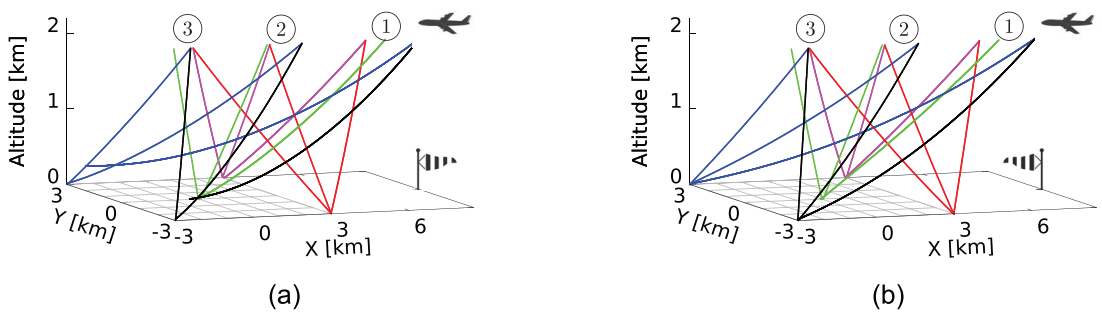


FIG. 10. (Color online) Direct eigenrays traced between vehicle emission time positions and the microphones located at the corners and the center of the ground area in the clear day condition for the wind blowing against the flight direction (a) and along the flight direction (b).

https://doi.org/10.1121/10.0005733

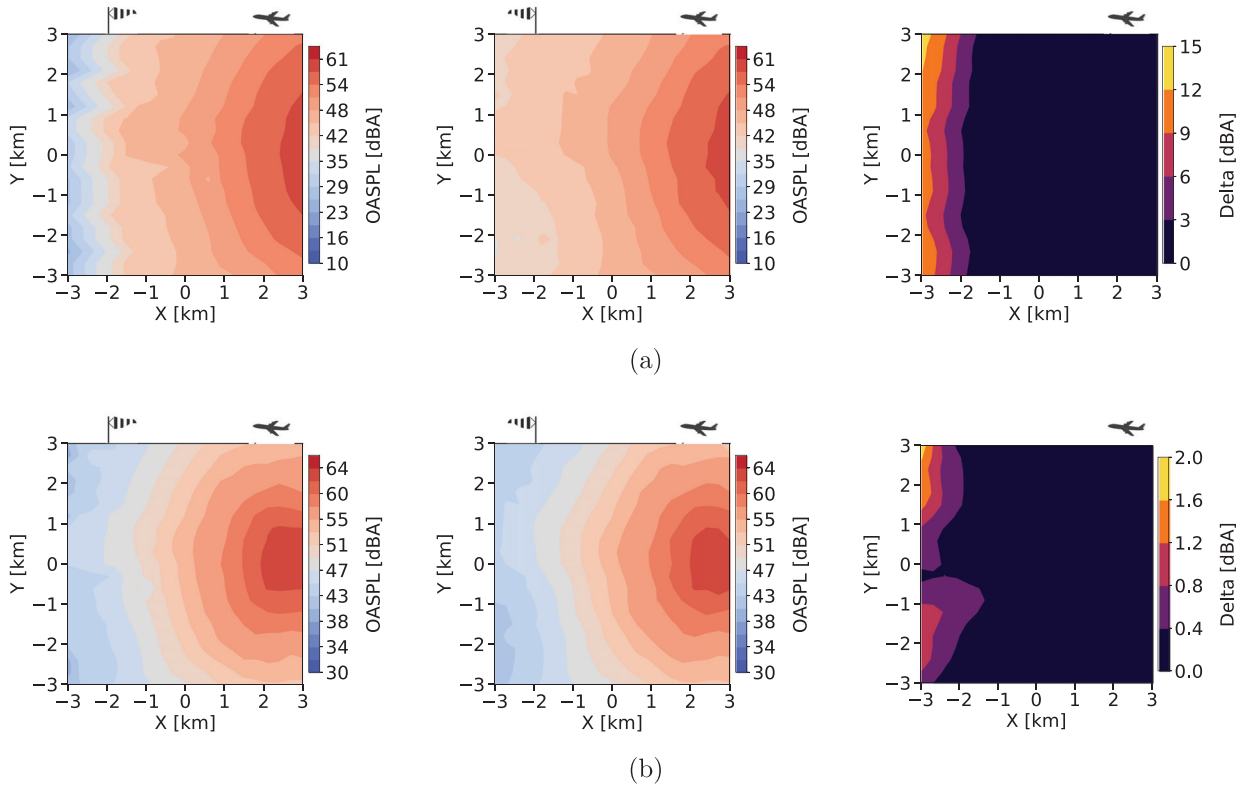


FIG. 11. (Color online) On-ground noise footprints at control point A (a) and B (b) in the clear day with wind directions against the flight direction, along the flight direction, and field difference between them.

## ACKNOWLEDGMENTS

This work was financially supported by Airbus Defence and Space. The authors are grateful for this support.

Ahearn, M., Boeker, E., Gorshkov, S., Hansen, A., Hwang, S., Koopmann, J., Malwitz, A., Noel, G., Reherman, C. N., Senzig, D. A., Solman, G. B., Tosa, Y., Wilson, A., Zubrow, A., Didyk, N., DiPardo, J., Grandi, F., Majeed, M., Bernal, J., Dinges, E., Rickel, D., Yaworski, M., Hall, C., and Augustine, S. (**2016**). "Aviation environmental design tool (AEDT): Technical manual, version 2b, service pack 3," Technical Report, Federal Aviation Administration, Washington, DC.

Antcliff, K. R., Moore, M. D., and Goodrich, K. H. (**2016**). "Silicon Valley as an early adopter for on-demand civil VTOL operations," in *Proceedings of the 16th AIAA Aviation Technology, Integration, and Operations Conference*, June 13–17, Washington, DC, pp. 3466–3483.

Arntzen, M., Rizzi, S. A., and Visser, H. G. (**2012**). "A framework for simulation of aircraft flyover noise through a non-standard atmosphere," in *Proceedings of the 18th AIAA/CEAS Aeroacoustics Conference*, June 4–7, Colorado Springs, CO, p. 17.

Basner, M., and McGuire, S. (**2018**). "WHO environmental noise guidelines for the European region: A systematic review on environmental noise and effects on sleep," Int. J. Environ. Res. Public Health **15**(3), 519–564.

Browne, R., Munt, R., Simpson, C., and Williams, T. (**2004**). "Prediction of helicopter noise contours for land use planning," in *Proceedings of the 10th AIAA/CEAS Aeroacoustics Conference*, May 10–12, Manchester, UK, pp. 2811–2822.

Casalino, D. (**2003**). "An advanced time approach for acoustic analogy predictions," J. Sound Vib. **261**(4), 583–612.

Casalino, D., Barbarino, M., and Visingardi, A. (**2011**). "Simulation of helicopter community noise in complex urban geometry," AIAA J. **49**(8), 1614–1624.

Casalino, D., van der Velden, W. C., and Romani, G. (**2019a**). "Community noise of urban air transportation vehicles," in *Proceedings of the AIAA Scitech 2019 Forum*, January 7–11, San Diego, CA, pp. 1834–1851.

Casalino, D., van der Velden, W. C., Romani, G., and Gonzalez-Martino, I. (**2019b**). "Aeroacoustic analysis of urban air operations using the LB/VLES method," in *25th AIAA/CEAS Aeroacoustics Conference*, May 20–23, Delft, The Netherlands, pp. 2662–2673.

Conner, D. A., and Page, J. A. (**2002**). "A tool for low noise procedures design and community noise impact assessment: The rotorcraft noise model (RNM)," in *Proceedings of Heli Japan*, November 11–13, Tochigi, Japan.

de Moraes Calazan, R., and Rodríguez, O. C. (**2018**). "Simplex based three-dimensional eigenray search for underwater predictions," J. Acoust. Soc. Am. **143**(4), 2059–2065.

ECAC (**2016**). "ECAC.CEAC Doc. 29. report on standard method of computing noise contours around civil airports. Volume 2: Technical guide," Technical Report, European Civil Aviation Conference, Neuilly-sur-Seine, France.

Evrard, A.-S., Bouaoun, L., Champelovier, P., Lambert, J., and Laumon, B. (**2015**). "Does exposure to aircraft noise increase the mortality from cardiovascular disease in the population living in the vicinity of airports? Results of an ecological study in France," Noise Health **17**(78), 328–336.

Farassat, F., and Succi, G. P. (**1982**). "The prediction of helicopter discrete frequency noise," Am. Helicopter Soc. **1982**, 497–507.

Franke, S. J., and Swenson, G. W. (**1989**). "A brief tutorial on the fast field program (FFP) as applied to sound propagation in the air," Appl. Acoust. **27**, 203–215.

Gabillet, Y., Schroeder, H., Daigle, G. A., and L'Espérance, A. (**1993**). "Application of the gaussian beam approach to sound propagation in the atmosphere: Theory and experiments," J. Acoust. Soc. Am. **93**(6), 3105–3116.

Gennaretti, M., Serafini, J., Bernardini, G., Castorrini, A., De Matteis, G., and Avanzini, G. (**2016**). "Numerical characterization of helicopter noise hemispheres," Aerosp. Sci. Technol. **52**, 18–28.

Gervais, M., Gareton, V., Dummel, A., and Heger, R. (**2010**). "Validation of EC130 and EC135 environmental impact assessment using HELENA," in *Proceedings of the American Helicopter Society 66th Annual Forum*, May 11–13, Phoenix, AZ.

Ghinet, S., Price, A., Daigle, G. A., Stinson, M. R., Grewal, A., and Wickramasinghe, V. (**2019**). "Atmospheric propagation of aircraft acoustic signature from high altitude," in *INTER-NOISE and NOISE-CON Congress and Conference Proceedings*, June 16–19, Madrid, Spain, Vol. 259, pp. 4654–4665.

Gilbert, K. E., and White, M. J. (**1989**). "Application of the parabolic equation to sound propagation in a refracting atmosphere," J. Acoust. Soc. Am. **85**(2), 630–637.

Gopalan, G. (**2004**). "Quasi-static acoustic mapping of helicopter blade-vortex interaction noise," Ph.D. dissertation, University of Maryland, College Park, MD.

Greenwood, E. (**2011**). "Fundamental rotorcraft acoustic modelling from experiments (FRAME)," Ph.D. dissertation, University of Maryland, College Park, MD.

Greenwood, E. (**2017**). "Helicopter flight procedures for community noise reduction," in *AHS International 73rd Annual Forum Proceedings*, May 9–11, Fort Worth, TX.

Guntzer, F., Spiegel, P., and Lummer, M. (**2009**). "Genetic optimizations of EC-135 noise abatement flight procedures using an aeroacoustic database," in *Proceedings of the 35th European Rotorcraft Forum*, September 22–25, Hamburg, Germany.

Guski, R., Schreckenberg, D., and Schuemer, R. (**2017**). "WHO environmental noise guidelines for the European region: A systematic review on environmental noise and annoyance," Int. J. Environ. Res. Public Health **14**(12), 1539–1578.

Hartjes, S., and Visser, H. G. (**2019**). "Optimal control approach to helicopter noise abatement trajectories in nonstandard atmospheric conditions," J. Aircraft **56**(1), 43–52.

Holden, J., and Goel, N. (**2016**). "Fast-forwarding to a future of on-demand urban air transportation," Uber Elevate, https://www.uber.com/elevate.pdf (Last viewed February 2021).

Klug, H. (**1991**). "Sound-speed profiles determined from outdoor sound propagation measurements," J. Acoust. Soc. Am. **90**(1), 475–481.

Lagarias, J. C., Reeds, J. A., Wright, M. H., and Wright, P. E. (**1998**). "Convergence properties of the Nelder–Mead simplex method in low dimensions," SIAM J. Optim. **9**(1), 112–147.

Lamancusa, J. S., and Daroux, P. A. (**1993**). "Ray tracing in a moving medium with two-dimensional sound speed variation and application to sound propagation over terrain discontinuities," J. Acoust. Soc. Am. **93**, 1716–1726.

Lucas, M. J., and Marcolini, M. A. (**1997**). "Rotorcraft noise model," J. Acoust. Soc. Am. **101**(5), 3188–3188.

Munt, R. M., Browne, R. W., Pidd, M., and Williams, T. (**2001**). "A measurement and prediction method for determining helicopter noise contours," in *Proceedings of the 27th European Rotorcraft Forum*, May 11–14, Moscow, Russia.

Nassur, A.-M., Lefèvre, M., Laumon, B., Léger, D., and Evrard, A.-S. (**2019**). "Aircraft noise exposure and subjective sleep quality: The results of the Debats study in France," Behav. Sleep Med. **17**(4), 502–513.

Nelder, J. A., and Mead, R. (**1965**). "A simplex method for function minimization," Comput. J. **7**(4), 308–313.

Ostashev, V. E., and Wilson, D. K. (**2015**). *Acoustics in Moving Inhomogeneous Media*, 2nd ed. (CRC, New York), Chaps. 1 and 3.

Panosfsky, H., and Dutton, J. (**1984**). *Atmospheric Turbulence: Models and Methods for Engineering Applications*, 1st ed. (Wiley, New York), Chap. 6.

Parry, J. A., Van Renterghem, T., Horoshenkov, K. V., and Williams, D. P. (**2020**). "Statistical analysis of sound propagation in uncertain, refracting and turbulent atmospheres," available at https://www.jordanparry.uk/files/AppAcou_UncertainInhomoPropa.pdf.

Pierce, A. D. (**2019**). *Acoustics: An Introduction to Its Physical Principles and Applications*, 3rd ed. (Springer, New York), Chap. 8.

Rizzi, S., Huff, D., Boyd, D., Bent, P., Henderson, B., Pascioni, K., Sargent, C., Josephson, D., Marsen, M., He, H., and Snider, R. (**2020**). "Urban air mobility noise: Current practice, gaps, and recommendations," Technical Report, NASA Langley Research Center, Hampton, VA.

Salomons, E. M. (**2001**). *Computational Atmospheric Acoustics* (Springer Science & Business Media, Berlin), p. 335.

Seeley, B. A. (**2017**). "Regional sky transit III: The primacy of noise," in *Proceedings of the 55th AIAA Aerospace Sciences Meeting*, January 9–13, Grapevine, TX.

Shan, X., Yuan, X., and Chen, H. (**2006**). "Kinetic theory representation of hydrodynamics: A way beyond the Navier–Stokes equation," J. Fluid Mech. **550**, 413–441.

Stull, R. B. (**1988**). *An Introduction to Boundary Layer Meteorology* (Springer Science & Business Media, Berlin), Chap. 9.

Van Kempen, E., Casas, M., Pershagen, G., and Foraster, M. (**2018**). "WHO environmental noise guidelines for the European region: A systematic review on environmental noise and cardiovascular and metabolic effects: A summary," Int. J. Environ. Res. Public Health **15**(2), 379–438.

Vascik, P. D., and Hansman, R. J. (**2017**). "Evaluation of key operational constraints affecting on-demand mobility for aviation in the los angeles basin: Ground infrastructure, air traffic control and noise," in *Proceedings of the 17th AIAA Aviation Technology, Integration, and Operations Conference*, June 5–9, Denver, CO, pp. 3084–3104.

Vascik, P. D., and Hansman, R. J. (**2018**). "Scaling constraints for urban air mobility operations: Air traffic control, ground infrastructure, and noise," in *Proceedings of the 2018 Aviation Technology, Integration, and Operations Conference*, June 25–29, Atlanta, Georgia, pp. 3849–3874.

Yin, J., Spiegel, P., and Buchholz, H. (**2007**). "Towards noise abatement flight procedure design: DLR rotorcraft noise ground footprints model and its validation," J. Am. Helicopter Soc. **52**(2), 90–98.